THE ASTROPHYSICAL JOURNAL, 376:278–288, 1991 July 20

OBSERVATIONS OF SCORPIUS X-1 WITH *IUE*: ULTRAVIOLET RESULTS FROM A MULTIWAVELENGTH CAMPAIGN

S. D. VRTILEK,[1] W. PENNINX,[2] J. C. RAYMOND,[1] F. VERBUNT,[3] P. HERTZ,[4] K. WOOD,[4]
W. H. G. LEWIN,[5] AND K. MITSUDA[6]

Received 1990 September 28; accepted 1991 January 21

ABSTRACT

We present ultraviolet results from a multiwavelength campaign on the low-mass X-ray binary Sco X-1. The ultraviolet observations were obtained with the *International Ultraviolet Explorer* (*IUE*) and coincided with X-ray observations taken with the Japanese satellite *Ginga* and other observations from numerous between the strengths of the UV continuum and line fluxes and the X-ray spectral states. Models predicting UV continuum emission from the X-ray–heated surface of the companion star and from an X-ray–illuminated accretion disk were adjusted for parameters intrinsic to Sco X-1 and fitted to the data. The data/model comparison shows the following for Sco X-1, as for Cyg X-2: (1) X-ray heating of the accretion disk is the dominant source of UV emission, (2) the mass accretion rate increases monotonically along the so-called Z-shaped curve in an X-ray color-color diagram, and (3) the disk structure does not change as a function of X-ray spectral state. The accretion disk model gives a best-fit outer disk radius of $(6.3 \pm 0.3) \times 10^{10}$ cm. Mass accretion rates range from $0.6 \times 10^{-8}\ M_\odot\ \mathrm{yr}^{-1}$ in the normal branch (NB) to $1.1 \times 10^{-8}\ M_\odot\ \mathrm{yr}^{-1}$ in the flaring branch (FB). The horizontal branch (HB) was not observed simultaneously in the UV and X-ray, but if the weakest state seen from earlier UV observations corresponds to the HB state, the mass accretion rate there is found to be $0.4 \times 10^{-8}\ M_\odot\ \mathrm{yr}^{-1}$.

Ultraviolet emission lines from He, C, N, O, and Si were detected; all increase in intensity from the HB to the FB state. A model in which emission lines are due to photoionization of the outer disk by the X-ray source was developed and gives good agreement with the line fluxes observed in each state.

The X-ray:UV:radio flux ratios of Sco X-1 measured at the lower vertex of the Z in the X-ray color-color diagram agree with those previously observed in five other X-ray binaries. We suggest that the flux at this vertex, which several theories identify with an accretion rate at the Eddington limit, may be used as a standard candle; the distance to Sco X-1 would then be 2.0 ± 0.5 kpc.

Subject headings: stars: individual (Scorpius X-1) — ultraviolet: spectra — X-rays: binaries

1. INTRODUCTION

Sco X-1 is classified as a Z source, a subclass of low-mass X-ray binaries (LMXBs; Hasinger & van der Klis 1989). It has an orbital period, derived from photometry (Gottlieb, Wright, & Liller 1975) and confirmed with radial velocity measurements (Cowley & Crampton 1975), of 0.787 days. Its optical companion, V818 Sco, is a 13th mag star with excess UV emission. The optical spectra show a very blue continuum with weak, broad emission lines (He, C, N, O, and Si), in addition to prominent and highly variable He II λ4686 and Balmer series emission (Crampton et al. 1976); the optical emission is assumed to originate from an accretion disk, since no stellar signature is seen. The UV spectra show variable emission lines due to O, N, Si, C, and He with no dependence on orbital phase (Willis et al. 1980; Kallman, Raymond, & Vrtilek 1991, hereafter KRV91).

The X-ray spectra of Z sources show three distinct states (as determined by X-ray hardness ratio measurements): these are referred to as horizontal branch (HB), where the spectral hardness remains almost constant during large excursions in source intensity; the normal branch (NB), where the hardness ratio increases with source intensity; and the flaring branch (FB), where both hardness ratio and intensity fluctuate erratically. When plotted on a X-ray color-color diagram these three branches form a Z-shaped curve (Hasinger 1987; Garcia 1987).

Each branch of the Z shows a distinctive pattern of quasi-periodic oscillations (QPOs; for a review, see van der Klis 1989). The HB observations show QPOs with frequency (20–50 Hz) correlated with intensity (Hasinger 1987; Stella 1988); three components of excess power are visible: a QPO peak, a broad hump between 0.1 and 10 Hz, called low-frequency (6 Hz) noise (LFN); and a steep power law component below 0.1 Hz, denoted very low frequency noise (VLFN). On the NB, QPOs have low frequencies which mostly do not change noticeably with source intensity and are not accompanied by LFN; however, VLFN is always present (Norris & Wood 1987). During the FB, the QPOs increase in frequency (from $\sim$6 to 20–50 Hz) and then dissolve into a continuum of excess broad power continuum (Priedhorsky et al. 1986; Penninx et al. 1990a; Hasinger et al. 1990).

An outstanding problem with models for Z sources has been lack of knowledge of the mass transfer rate during the QPO phenomenon. If mass transfer is a continuous function of the position along the Z-track, on at least one branch the mass transfer is anticorrelated with X-ray flux. A multiwavelength

[1] Harvard-Smithsonian Center for Astrophysics, 60 Garden Street, Cambridge, MA 02138.
[2] Astronomical Institute "Anton Pannekoek," University of Amsterdam, Roetersstraat 15, 1018 WB, Amsterdam, The Netherlands.
[3] Astronomical Institute, University of Utrecht.
[4] Naval Research Laboratory, Code 4121.5, Washington, DC 20375.
[5] Center for Space Research, Massachusetts Institute of Technology, Cambridge, MA 02139.
[6] Institute of Space and Astronautical Studies, 3-1-1 Yoshinodai, Sagamihara-shi, Kanagawa-ken, 229 Japan.

study to address this issue has been conducted recently on the LMXB, Cyg X-2. Using data from this study Hasinger et al. (1990) and Vrtilek et al. (1989, 1990) found an interesting relationship between the three X-ray spectral states and the UV emission observed by *IUE*: the UV continuum strength and line strength both increase monotonically along the Z-shaped curve. Along the horizontal branch the UV continuum is low and line emission weak, on the normal branch UV continuum is stronger and line emission more apparent; and in the flaring branch both UV continuum and line emission are strong. Models predicting UV continuum emission from the X-ray–heated surface of the companion star and from an X-ray–illuminated accretion disk were developed. The X-ray–heated disk is found to be the dominant source of UV emission with the mass accretion rate following the UV flux and increasing monotonically along the Z.

Sco X-1 is the brightest X-ray point source in the sky and also a very bright UV source (with a continuum flux of $\sim 10^{-10}$ ergs cm^{-2} s^{-1}) as previously observed by *IUE* (Willis et al. 1980). Sco X-1 and Cyg X-2 are the only Z sources that are visible optically (the remaining four have large interstellar absorption). The success of the Cyg X-2 multiwavelength campaign quickly led to a similar campaign focused on Sco X-1. Previous observations of Sco X-1 with *IUE* showed no obvious correlations of line emission with phase, but significant changes in line emission occur as the source changes in UV and optical brightness (Willis et al. 1980); our simultaneous UV/X-ray observations show that these changes correspond to different X-ray spectral states.

Because of its brightness in the X-rays Sco X-1 is difficult to observe with proportional counters such as those carried by *Ginga*. For this campaign, Hertz et al. (1991) offset the *Ginga* detectors in order to observe Sco X-1 without saturation, providing an unusual opportunity to obtain simultaneous X-ray/UV observations of the brightest nonsolar X-ray source in the sky, and the brightest UV emitter among LMXBs. Our observations constitute the first *simultaneous* ultraviolet and X-ray spectra of Sco X-1 with sufficient spectral and temporal resolution to resolve the X-ray spectral states and to detect the QPOs. They show that the Sco X-1 ultraviolet/X-ray/radio behavior is analogous to that of Cyg X-2. The startling similarity in behavior of the two sources in addition to the model-dependent assumption that the lower, "soft," vertex of the Z is at the Eddington limit implies that one may be able to use the Z sources as a standard candle to determine their distances (Penninx 1989).

The UV observations are described in § 2; the radio, optical, and X-ray observations will be described elsewhere (Hjellming et al. 1990b; van Paradijs et al. 1991; Hertz et al. 1991). In § 3 we compare the data and models predicting UV emission from the X-ray–heated surface of the accretion disk; in § 4 we present some diagnostics based on the UV emission lines observed. An analysis of the reddening and distance to Sco X-1 is presented in § 5, and a discussion of our results and the implications for models of Z-sources are presented in § 6.

2. OBSERVATIONS

The UV data discussed here were obtained mostly during an international multiwavelength campaign conducted in March of 1989 and involving groups from Japan, Europe, and the United States. In the two days of the multiwavelength campaign we obtained a total of 31 *IUE* spectra covering two orbital cycles. Eighteen used the short-wavelength camera (SWP) which covers the 1150–2000 Å band, and 13 used the long-wavelength camera (LWP) which covers the 1900–3200 Å band. The exposures ranged from 25 to 50 minutes in duration.

Table 1, gives a log of the observations. The *IUE* instrument, described in detail by Boggess et al. (1978a, b), is a UV echelle spectrometer. It was used in the low-dispersion mode ($\Delta\lambda \approx$ 6 Å) with the large aperture (10″ × 20″) to ensure photometric accuracy. The camera sequence number, Julian Date (JD) of the start of the exposure, total exposure time, and binary phases using the ephemeris of Crampton et al. (1976) are also listed. All *IUE* observations of Sco X-1 were reduced uniformly using the Gaussian extraction technique described by Urry & Reichert (1988). Although this technique, developed principally for optimal information recovery from weak sources, is not necessary in the case of Sco X-1, the improvement in signal-to-noise ratio for weak spectral features justifies the added effort to apply this method (see § 5). An improvement by a factor of 2–3 in signal-to-noise ratio for weak features such as the O IV λ1370 and He II λ1640 is obtained. The extracted spectra were calibrated using the absolute energy scale determined by Bohlin et al. (1980).

The simultaneous X-ray observations using the *Ginga* satellite captured two spectral branches (NB and FB) and their associated QPO modes (Hertz et al. 1991). The X-ray state was determined by producing a color-color diagram where the soft hardness ratio was determined by dividing the 4.6–6.9 keV flux by that of the 2.3–4.6 keV flux, and the hard hardness ratio by dividing the 9.2–18.4 keV flux by that of the 6.9–9.2 keV flux. The X-ray light curve with the two spectral states designated are shown in Figure 1; the corresponding UV fluxes are also depicted. We note that the HB state of Sco X-1 has been observed only once in X-ray observations (Hasinger, Priedhorsky, & Middleditch 1989). The optical continuum flux is found to be directly correlated with UV flux (van Paradijs et al. 1991). The radio observations showed quiescent emission with

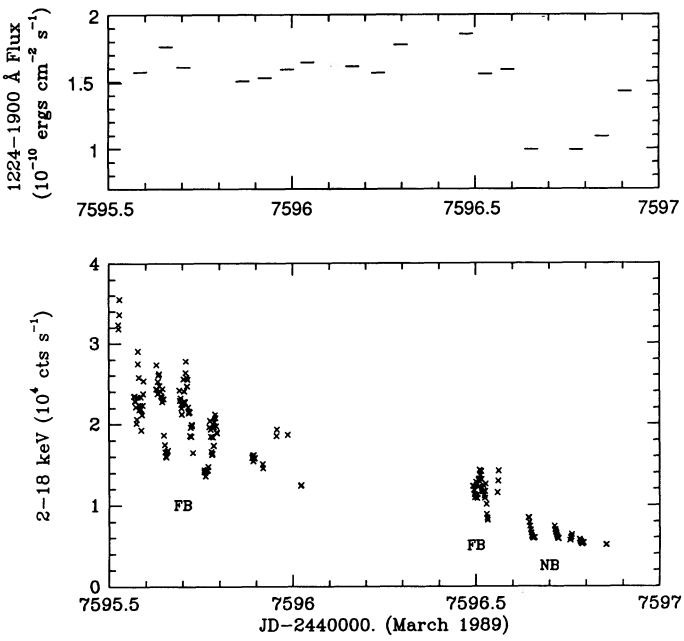

FIG. 1.—X-ray light curves (from *Ginga*) and UV coverage (from *IUE*), with average fluxes noted for the SWP exposures.

TABLE 1

SCORPIUS X-1/V818 SCORPII *IUE* OBSERVATIONS

UT Date of Observation (1989)	Sequence	Start Time	Exposure (minutes)	Binary Phase at Start of Observation
Mar 9	SWP 35724	JD 2,447,595.517	45	0.534
	LWP 15158	JD 2,447,595.553	40	0.579
	SWP 35725	JD 2,447,595.587	40	0.623
Mar 10	LWP 15159	JD 2,447,595.620	30	0.664
	SWP 35726	JD 2,447,595.656	40	0.710
	SWP 35727	JD 2,447,595.704	40	0.771
	SWP 35728	JD 2,447,595.865	40	0.976
	LWP 15160	JD 2,447,595.901	25	0.021
	SWP 35729	JD 2,447,595.926	40	0.053
	LWP 15161	JD 2,447,595.959	30	0.095
	SWP 35730	JD 2,447,595.987	40	0.131
	LWP 15162	JD 2,447,596.020	25	0.173
	SWP 35731	JD 2,447,596.042	40	0.200
	SWP 35732	JD 2,447,596.165	45	0.357
	LWP 15163	JD 2,447,596.213	25	0.418
	SWP 35733	JD 2,447,596.236	45	0.447
	LWP 15164	JD 2,447,596.273	25	0.494
	SWP 35734	JD 2,447,596.297	40	0.524
	LWP 15165	JD 2,447,596.330	25	0.566
	SWP 35735	JD 2,447,596.475	40	0.750
Mar 11	LWP 15166	JD 2,447,596.509	25	0.794
	SWP 35736	JD 2,447,596.528	38	0.818
	LWP 15167	JD 2,447,596.565	25	0.865
	SWP 35737	JD 2,447,596.589	40	0.895
	LWP 15168	JD 2,447,596.630	25	0.947
	SWP 35738	JD 2,447,596.653	50	0.977
	SWP 35739	JD 2,447,596.775	50	0.132
	LWP 15169	JD 2,447,596.817	25	0.185
	SWP 35740	JD 2,447,596.845	50	0.220
	LWP 15170	JD 2,447,596.885	25	0.271
	SWP 35741	JD 2,447,596.907	40	0.299

NOTE.—Orbital phases are calculated using the ephemeris of Crampton et al. 1976: JD = 2,442,565.741 for phase 0.0 and a period of 0.787313 ± 0.000001 days.

increasing radio fluxes from FB to NB (Hjellming et al. 1990b) in agreement with the behavior seen in GX 17+2 (Penninx et al. 1988) and Cyg X-2 (Hjellming et al. 1990a).

Table 2 gives the 1224–1986 Å continuum and line fluxes for both the new *IUE* observations discussed here as well as for 10 SWP observations taken previously (KRV91). The long-wave length spectra obtained with the LWP are not included in Table 2 as they show only very weak features aside from the absorption feature at 2200 Å attributed to interstellar absorption. We note that all *IUE* spectra taken previous to this campaign have been analyzed by KRV91 using the normal RDAF extraction procedure (rather than the Gaussian extraction). The overlapping exposures that we present (in order to show what we believe are HB branch observations in the UV which were not detected in the current campaign) should also serve to allow comparison between the two extractions. The continuum is determined by integrating the flux from 1224 to 1986 Å and subtracting the contribution due to known lines and hits (sharp bright spots in the image caused by radioactive decay of cosmic-ray hits). In the 28 SWP exposures presented, emission lines due to He, C, N, O, and Si are detected. The fluxes of the line features are strongly correlated with the continuum fluxes (Fig. 2; see also KRV91), but the correlation of either continuum or line fluxes with binary phase is weak (Fig. 3). The dependence of the UV flux on X-ray spectral state is apparent in Figure 2, with both the continuum and line fluxes increasing from the HB to the FB states.

3. AN X-RAY–ILLUMINATED ACCRETION DISK

The ultraviolet emission we observed from Sco X-1 is too high to be attributed to direct emission from the optical star or to viscous heating of the disk. Since no stellar spectral signature is seen for V818 Scorpii, we are unable to compute the effects of X-ray heating on the companion star. For Cyg X-2 we were able to show that emission from the X-ray–heated companion star is negligible in the ultraviolet (Vrtilek et al. 1990); however, the separation of the two stars in Cyg X-2, which has an orbital period of 9.8 days, is large, about 2×10^{12} cm. In Her X-1 this separation is about 2×10^{11} cm, and X-ray heating of the companion star plays a large role (Howarth & Wilson 1983). For Sco X-1 with a separation of 6×10^{10} cm, one would expect this to be even a greater effect. However, no orbital variation in the ultraviolet continuum flux (as would be expected if the companion showed X-ray heating effects) is observed, although optical photometry shows orbital effects (Gottlieb, Wright, & Liller 1975). We conclude that the X-ray–heated companion star is too cool or small to be important in the ultraviolet.

The simple model for X-ray heating of the accretion disk developed by us earlier for application to Cyg X-2 (Vrtilek et al. 1990) was adapted for the Sco X-1 system parameters. A distance to Sco X-1 of 2.0 kpc and an inclination of 30° are assumed following the conclusions of Crampton et al. (1976). An $E(B-V)$ of 0.3 derived from fits to the 2200 Å feature in the

TABLE 2

ULTRAVIOLET CONTINUUM AND LINE FLUXES

DATE OF OBSERVATION	SEQUENCE NUMBER	X-RAY STATE	BINARY PHASE	CONTINUUM AT 1200 Å (10^{-12} ergs cm^{-2} s^{-1} Å)	1224–1986 Å FLUX (10^{-11} ergs cm^{-2} s^{-1})			FLUX IN LINE (10^{-11} ergs cm^{-2} s^{-1})					
					Total	Continuum	Line	N V λ1240	O V λ1370	Si V λ1400	C IV λ1545	He II λ1640	N IV λ1714
A. *IUE* Data from Current Campaign													
1989 Mar 9	35724	FB	0.83	0.18	15.97	14.93	1.05	0.408	0.084	0.121	0.350	0.047	0.044
	35725	FB	0.92	0.20	16.88	15.73	1.15	0.495	0.079	0.083	0.392	0.062	0.036
1989 Mar 10	35726	FB	0.00	0.17	18.70	17.61	1.09	0.489	0.055	0.073	0.365	0.060	0.050
	35727	FB	0.07	0.21	17.04	16.09	0.95	0.386	0.026	0.040	0.407	0.042	0.044
	35728	FB	0.30	0.21	15.98	15.05	0.89	0.330	0.048	0.052	0.350	0.055	0.057
	35729	FB	0.35	0.21	16.19	15.28	0.91	0.390	0.076	0.001	0.366	0.031	0.045
	35730	FB	0.43	0.21	17.00	15.93	1.07	0.460	0.036	0.083	0.385	0.034	0.067
	35731	FB	0.50	0.17	17.54	16.45	1.09	0.499	0.062	0.051	0.386	0.047	0.043
	35732	FB	0.65	0.19	17.26	16.15	1.11	0.417	0.076	0.119	0.414	0.048	0.036
	35733	FB	0.74	0.18	16.74	15.66	1.09	0.459	0.150	0.247	0.337	0.056	0.045
	35734	FB	0.82	0.25	19.10	17.77	1.33	0.369	0.109	0.068	0.363	0.059	0.091
	35735	FB	0.04	0.25	19.79	18.57	1.22	0.414	0.101	0.158	0.425	0.065	0.058
1989 Mar 11	35736	FB	0.11	0.18	16.62	15.56	1.06	0.457	0.059	0.118	0.326	0.056	0.041
	35737	FB	0.19	0.23	16.95	15.89	1.06	0.351	0.084	0.128	0.402	0.048	0.045
	35738	NB	0.27	0.14	10.71	9.94	0.77	0.276	0.017	0.060	0.343	0.037	0.038
	35739	NB	0.43	0.13	10.74	9.91	0.83	0.291	0.014	0.090	0.362	0.050	0.024
	35740	NB	0.51	0.13	11.80	10.93	0.87	0.333	0.045	0.059	0.348	0.052	0.028
	35741	NB	0.59	0.17	15.27	14.27	0.99	0.380	0.074	0.074	0.397	0.029	0.037
B. *IUE* Data Taken Previous to This Campaign													
1984 Mar 18	22512	FB	0.86	0.20	19.86	18.59	1.27	0.422	0.098	0.152	0.473	0.071	0.053
	22514	FB	1.00	0.21	19.62	18.39	1.23	0.401	0.119	0.187	0.412	0.053	0.061
1984 Aug 3	23592	FB	0.11	0.17	15.60	14.38	1.22	0.342	0.087	0.160	0.485	0.083	0.067
1984 Mar 14	22485	NB	0.80	0.12	9.93	9.37	0.55	0.175	0.031	0.060	0.229	0.029	0.030
	22486	NB	0.91	0.15	12.77	12.00	0.77	0.232	0.069	0.079	0.311	0.029	0.045
1984 Jul 21	23480	NB	0.58	0.13	12.29	11.21	1.08	0.345	0.054	0.118	0.449	0.057	0.061
1984 Mar 6	22424	HB	0.42	0.10	8.75	8.18	0.57	0.161	0.049	0.064	0.245	0.024	0.023
1984 Aug 16	23702	HB	0.61	0.09	6.86	6.49	0.37	0.107	0.015	0.041	0.168	0.021	0.021
	23703	HB	0.67	0.08	7.33	6.94	0.39	0.134	0.023	0.041	0.145	0.017	0.026
	23704	HB	0.41	0.10	8.04	7.62	0.42	0.134	0.036	0.044	0.171	0.018	0.021

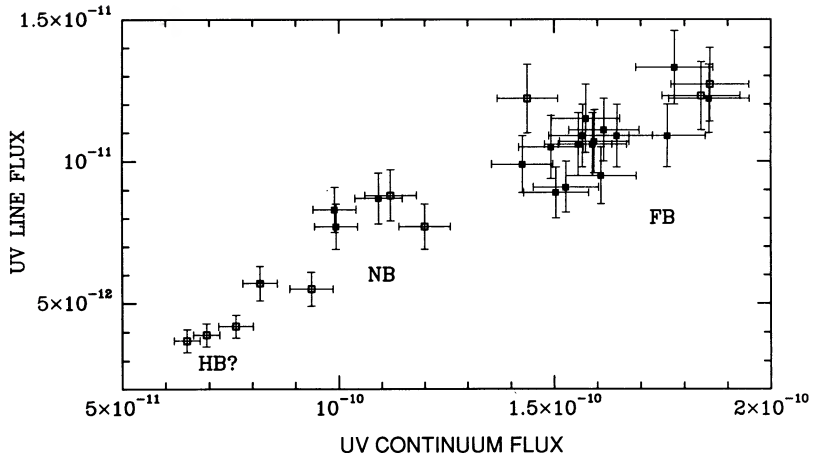

FIG. 2.—UV continuum flux vs. line flux in 1224–1986 Å band. Filled squares are values from current campaign as listed in Table 2A; open squares are values from *IUE* observations taken previous to this campaign as listed in Table 2B.

LWP spectra (Fig. 4) was used. Section 5 gives a detailed discussion of the distance and $E(B-V)$ determinations.

The ultraviolet emission from the accretion disk was computed with an improved version of the model constructed for Cen X-4 by Blair et al. (1984). The temperature as a function of radius is computed for a steady accretion disk with the mass transfer rate and outer radius as free parameters and the mass and radius of the central compact object held at 1.4 $M_\odot$ and 10^6 cm. The temperature is used to find the disk thickness as a function of radius. The X-ray luminosity $(1/2)GM\dot{M}/r_{ns}$ from the boundary layer where the disk encounters the neutron star (see Pringle 1981) is assumed to be radiated isotropically. We note that in the relativistic case the X-ray luminosity from the boundary layer may be closer to $(3/4)GM\dot{M}/r_{ns}$ (Paczyński 1987); hence, the mass accretion rates we compute may be overestimates. We compute the X-ray flux incident on the disk surface in each annulus, assume an albedo of 0.5, then compute a new temperature needed to radiate away the total locally generated accretion power and absorbed X-ray flux. The new temperature implies a new disk height, which changes the amount of incident X-ray flux. The temperature structure is iterated, being fitted to two power laws (the disk height of the illuminated disk varies as $r^{-3/7}$ and that of the unilluminated disk varies as $r^{-3/4}$) in radius at each iteration to control instabilities. The UV spectra are obtained by using stellar spectra at the same effective temperatures (S. Kenyon 1988, personal communication). These models give UV fluxes about a factor of 10 larger than would be obtained from models with the same accretion rates without X-ray heating. The assumption of steady state may not be entirely appropriate, in that the flow time through the disk is many days (for an α disk with $\alpha \approx 1$; Pringle 1981), while the X-ray illumination changes much more rapidly. To the extent that X-ray heating dominates, the

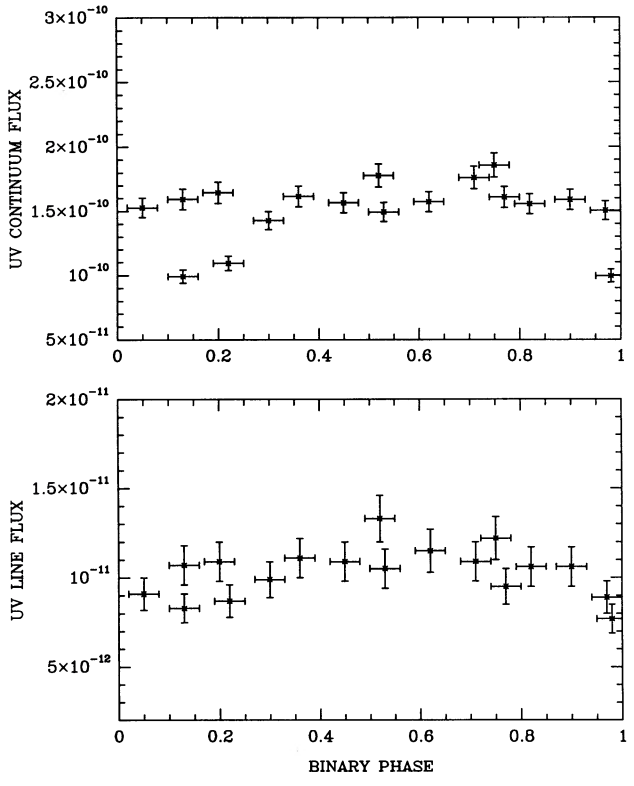

FIG. 3.—(*Top*) UV continuum flux vs. binary phase; (*bottom*) UV line flux vs. binary phase. Filled squares are values from current campaign as listed in Table 2A; open squares are values from *IUE* observations taken previous to this campaign as listed in Table 2B.

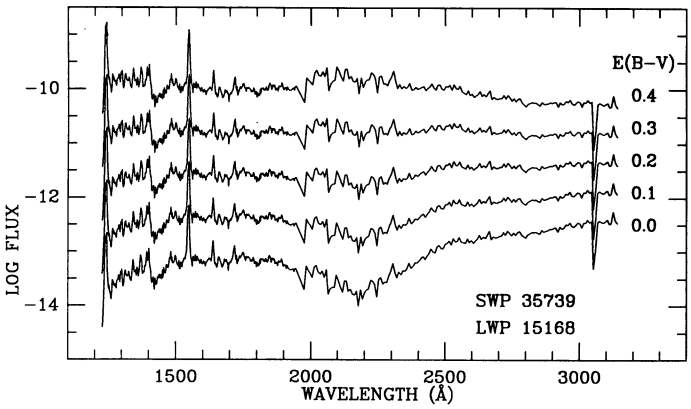

FIG. 4.—Sco X-1 dereddening. Merged (short-wavelength plus long-wavelength) *IUE* spectra from a NB state with different values of reddening correction applied using the extinction law of Seaton (1979).

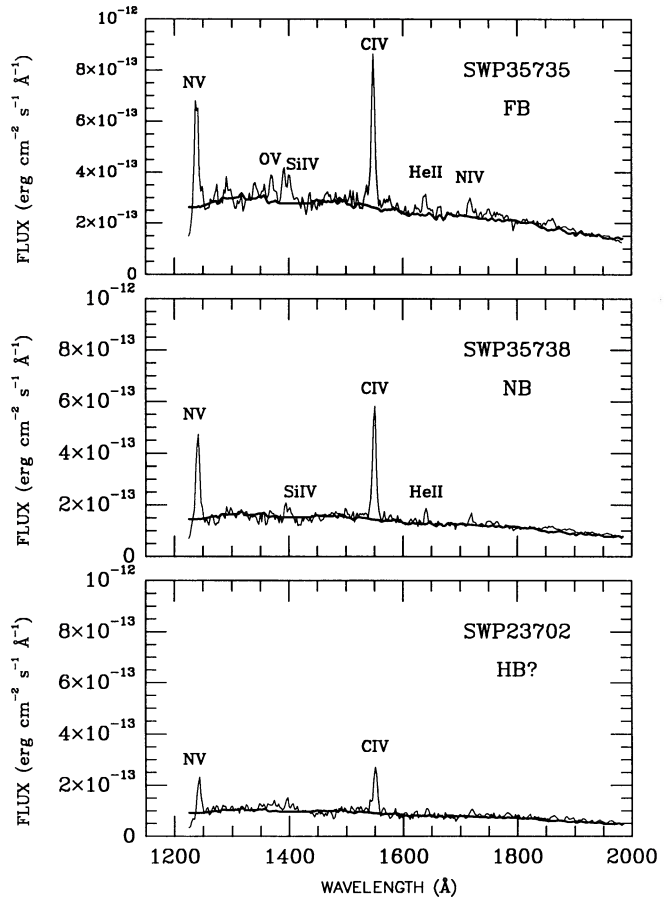

FIG. 5.—Three examples of *IUE* short-wavelength spectra showing the differences in spectral behavior during the three X-ray states: (*top*) flaring branch, (*middle*) normal branch, and (*bottom*) horizontal branch. The solid line shows the best-fit X-ray heated accretion disk model for the continuum. The HB requires a mass accretion rate of $0.6 \times 10^{-8}\ M_\odot\ \mathrm{yr}^{-1}$; the NB, $1.0 \times 10^{-8}\ M_\odot\ \mathrm{yr}^{-1}$; and the FB, $1.6 \times 10^{-8}\ M_\odot\ \mathrm{yr}^{-1}$.

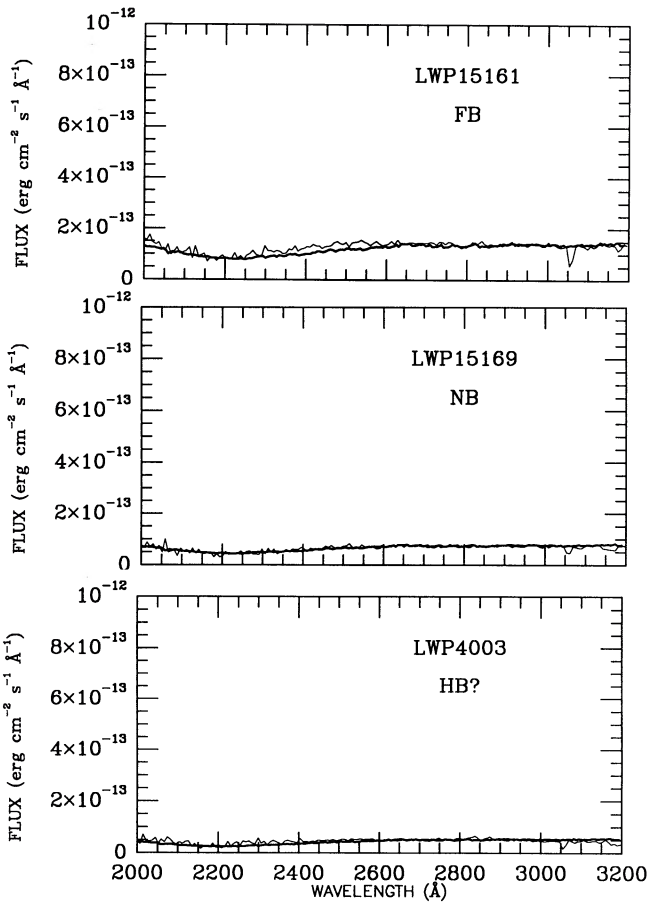

FIG. 6.—Three examples of *IUE* long-wavelength spectra of the three states HB, NB, and FB. These spectra are not corrected for reddening, and the absorption dip at 2200 Å is clearly visible. The solid line shows the best-fit X-ray–heated accretion disk model for the continuum. The HB requires a mass accretion rate of $0.6 \times 10^{-8}\ M_\odot\ \mathrm{yr}^{-1}$; the NB, $1.0 \times 10^{-8}\ M_\odot\ \mathrm{yr}^{-1}$; and the FB, $1.6 \times 10^{-8}\ M_\odot\ \mathrm{yr}^{-1}$.

response of the UV emission to changes in L_x is rapid, but it is possible that locally generated accretion power dominates when L_x drops quickly to low values (see Appendix in Vrtilek et al. 1990).

The best-fit parameter values of mass accretion rate and disk radius obtained using the X-ray–illuminated accretion disk model are given in Table 3. Examples for each of the three branches HB, NB, and FB are shown for the SWP (Fig. 5) and LWP (Fig. 6). The HB branch was *not* observed during this campaign: the UV spectra are inferred from *IUE* observations taken earlier. The best-fit outer disk radius was found to be 6×10^{10} cm for all three branches; spectra of smaller disks fell off too sharply at long wavelengths and those with larger radii produced too much optical emission (the FES on *IUE* recorded approximate optical V magnitudes ranging from 12.1 to 12.8 during our observations). UV observations that did not have simultaneous X-ray coverage are designated in Table 3 with "?" following the branch designation since the X-ray spectral state is deduced from the UV spectra.

The mass accretion rates for the three states range from $0.4 \times 10^{-8}\ M_\odot\ \mathrm{yr}^{-1}$ for the HB state to $1.2 \times 10^{-8}\ M_\odot\ \mathrm{yr}^{-1}$ for the FB state. The order of increasing mass accretion rate follows increasing UV continuum and line fluxes, which in turn follows the order HB, NB, FB as previously found for Cyg X-2. It is important to note that while the X-ray luminosity and disk radius are uncertain as a result of the assumed albedo, distance to the object, assumed isotropy of the X-ray emission, and the reddening, the *relative* X-ray luminosities required to fit different UV spectra should be correct. The central result of our investigation, an increase of about a factor 3.0 in mass accretion rate between HB and FB, is not sensitive to details of the model or the disk radius.

Many interpretations of the source spectral states for LMXBs assume that evolution from one spectral branch to another is associated with a change in the mass accretion rate. Both the optical and UV continuum fluxes play an important role in this context; as they are thought to originate from X-rays reprocessed by the accretion disk, their luminosity is expected to track the influx of X-rays and thus the accretion rate (Lyutyi & Sunyaev 1976). The UV flux is most likely to give direct information on the accretion disk and hence the accreting material, whereas the optical flux from the disk may be confused with the flux from the noncollapsed secondary (Willis et al. 1980). The UV is also a better indicator of the mass accretion rate than the X-ray flux; most models of LMXBs suggest geometries in which the observed X-ray flux is

TABLE 3

PARAMETER VALUES FOR ACCRETION DISK MODEL FITS TO SCORPIUS X-1

IUE Sequence Number	UV Flux[a] (10^{-11} ergs cm^{-2} s^{-1})	X-Ray State[b]	$\dot{M}$ (10^{-9} $M_\odot$ yr^{-1})
IUE Data from Current Campaign			
SWP 35724	14.93	FB	10.0
SWP 35725	15.73	FB	10.5
SWP 35726	17.61	FB?	10.0
SWP 35727	16.09	FB?	10.0
SWP 35728	15.05	FB	8.9
SWP 35729	15.28	FB	9.5
SWP 35730	15.93	FB	9.5
SWP 35731	16.45	FB	10.9
SWP 35732	16.15	FB?	10.9
SWP 35733	15.66	FB?	9.5
SWP 35734	17.77	FB?	11.1
SWP 35735	18.57	FB	11.1
SWP 35736	15.56	FB	9.5
SWP 35737	15.89	FB	9.5
SWP 35738	9.94	NB	5.8
SWP 35739	9.91	NB	5.8
SWP 35740	10.93	NB?	6.8
SWP 35741	14.27	NB?	8.4
LWP 15158	...	FB?	10.0
LWP 15159	...	FB	9.9
LWP 15160	...	FB	10.0
LWP 15161	...	FB	11.6
LWP 15162	...	FB	10.0
LWP 15163	...	FB?	10.0
LWP 15164	...	FB?	10.0
LWP 15165	...	FB?	10.5
LWP 15166	...	FB	10.5
LWP 15167	...	FB	10.5
LWP 15168	...	NB	7.9
LWP 15169	...	NB	6.3
LWP 15170	...	NB?	7.9
IUE Data Taken Previous to This Campaign			
SWP 22512	18.59	FB?	10.5
SWP 22514	19.92	FB?	10.5
SWP 23592	15.60	FB?	8.4
SWP 22485	9.93	NB?	5.3
SWP 22486	12.77	NB?	7.4
SWP 23480	12.29	NB?	7.4
SWP 22424	8.75	HB?	4.7
SWP 23702	6.86	HB?	3.7
SWP 23703	7.33	HB?	3.7
SWP 23704	8.04	HB?	4.2
LWP 2975	...	FB?	11.1
LWP 2976	...	FB?	11.1
LWP 3728	...	FB?	8.4
LWP 3729	...	FB?	9.5
LWP 3837	...	FB?	8.4
LWP 3931	...	FB?	8.4
LWP 2976	...	FB?	11.1
LWP 2917	...	NB?	6.8
LWP 2947	...	NB?	6.8
LWP 3930	...	NB?	5.3
LWP 2901	...	HB?	4.7
LWP 4003	...	HB?	4.2
LWP 4004	...	HB?	4.2
LWP 4005	...	HB?	4.7

[a] Integrated continuum flux from 1224 to 1986 Å for the SWP.

[b] Determined from *Ginga* color-color diagram. ? means no simultaneous X-ray data.

easily modulated by geometric effects (Begelman & McKee 1982 and references therein), e.g., by material interposed along the line of sight to the observer, or by accretion disk coronae, whereas the UV-emitting matter subtends a large solid angle as seen from the X-ray source and is therefore much less affected by geometric factors.

We conclude that the mass transfer rate can be determined from the flux level of the optical–ultraviolet spectrum. The uncertainty due to unknown details of the disk structure is about a factor of 2; the uncertainty due to unknown reddening is also about a factor of 2. The disk radius can be determined only within a factor of 2 from the slope of the ultraviolet spectrum, because this slope depends strongly on the assumed spectra of individual disk surface elements.

4. ULTRAVIOLET EMISSION LINES

Emission-line fluxes measured from spectra acquired in the current campaign and from 1984 are presented in Table 2. They show good agreement with the fluxes reported by Willis et al. (1980) and KRV91. However, the current study is able to obtain improved signal-to-noise ratios for weak features by utilizing the Gaussian extraction procedure which uses the known instrumental profile to reject noisy pixels. A further factor of 3 improvement in signal-to-noise ratio for weak features was obtained by taking the median of 13 SWP and nine LWP spectra from the FB state. Figure 7 shows the median averaged spectrum. Three lines in addition to those listed in Table 2 were definitely detected, C III λ1176, O IV λ1341, and O III λ3133 with fluxes of 6.2, 3.7, and 0.9 $\times$ 10^{-12} ergs cm^{-2} s^{-1}, respectively. The O III line is the strongest Bowen fluorescence line (Schachter, Filipenko, & Kahn 1989, hereafter

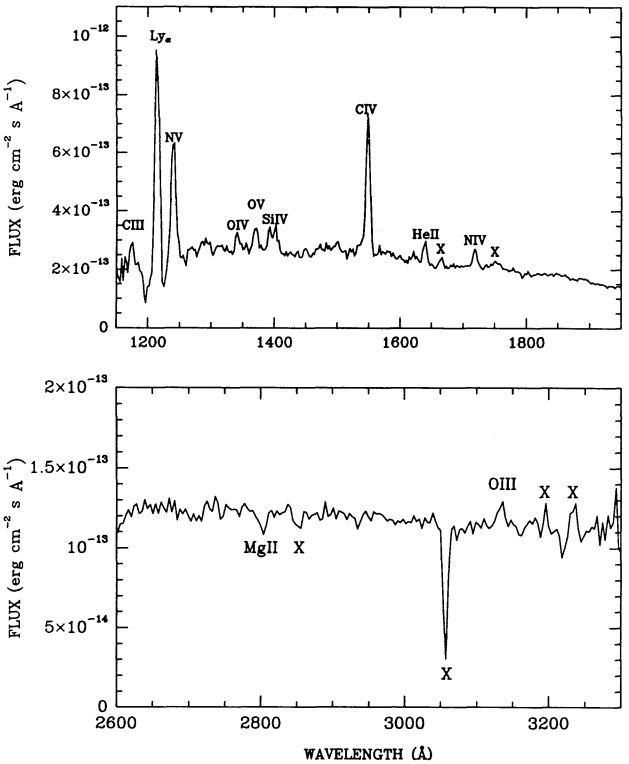

FIG. 7.—Averages of 14 SWP and 10 LWP spectra (all from the FB) showing weak line features not detectable with individual observations.

SFK89). Uncertainties in continuum placement, difficult to quantify, dominate the measurement errors for these lines. We estimate uncertainties of 10% for the strong lines and 20% for the weak lines. The features at 1662, 1750, 2850, 3060, and 3200 Å (marked with an X on Figure 7) are camera artifacts or reseau points (Bruegman & Crenshaw 1989). The feature at 3230 Å is unidentified, though an emission line at this wavelength shows up in a flaring branch spectrum shown by SFK89. The weak absorption feature at 2800 Å with an equivalent width of 1.0 Å is likely to be a real feature due to interstellar Mg.

To interpret the emission lines, we begin with a guess at their site of formation. The high dispersion profile of the C IV doublet shown in KRV91 indicates a line width of a few hundred kilometers per second, suggesting an origin in the outer accretion disk. It also shows an intensity ratio of 1:1 between the lines of the C IV doublet, indicating that the line formation is effectively optically thick. (The optically thin ratio would be 2:1.) Therefore radiative transfer must be incorporated into any model for the emission region.

Assuming that the emission lines arise in a hotter layer above the disk photosphere, there are several possibilities: X-ray heating (Compton heating and photoabsorption, as in Kallman & McCray 1982), viscous dissipation in the low-density layers above the photosphere (e.g., Shaviv & Wehrse 1986), or dissipation of the magnetic energy generated by the disk shear in analogy to solar X-ray–emitting loops (Galeev, Rosner, & Vaiana 1979). Once this question is answered, one can address the question of elemental abundances: Does the strength of N V relative to C IV (compared with cataclysmic variables, for example) require elemental abundances characteristic of CNO processing? An enhanced nitrogen abundance was inferred by Kahn, Seward, & Chlebowski (1984) from soft X-ray spectra.

As a first attempt to sort out these possibilities we compare the observed line fluxes with a model for the emission from the X-ray–illuminated surface of the accretion disk. The model will be described in detail by Raymond (1991). Briefly, we take the parameters from the calculations performed to fit the continuum, with $L_x = (1.2, 0.7, \text{and } 0.4) \times 10^{38}$ ergs s^{-1}, for the FB, NB, and HB states, respectively (corresponding to average mass accretion rates of 1.0, 0.7, and $0.4 \times 10^{-8}\ M_\odot$ yr^{-1} for the three states), and an outer disk radius of 6.3×10^{10} cm. The X-rays, assumed to be due to thermal bremsstrahlung at 10^8 K, strike the disk at a grazing angle.

The calculation iterates to find the ionization balance (photoionization + Auger ionization + collisional ionization = radiative + dielectronic recombination) and thermal balance (photoabsorption + Compton heating balances line cooling + recombination continuum + bremsstrahlung + Compton cooling) in a hydrostatic atmosphere. Abundant elements through iron are included (He = 10.93, C = 8.52, N = 7.96, O = 8.82, Ne = 7.92, Mg = 7.40, Si = 7.50, S = 7.20, Ar = 6.90, Ca = 6.30, Fe = 7.60 on a logarithmic scale where H = 12.0), and the atomic rates are largely as described by Mauche & Raymond (1987). Emission lines are computed in the escape probability approximation, with optical depths computed from the smaller of the Sobolev length due to Keplerian shear in the plane of the disk or the path length implied by the overlying column density of the ion in question. The line widths for the escape optical depth calculation are assumed to be dominated by turbulence at the sonic velocity. The model is similar to the model of Mobasher & Raine (1990) for the X-ray–illuminated surface of a disk in an active galactic nucleus, but with much higher densities, a small angle of incidence, no viscous dissipation in the line-emitting region, and a bremsstrahlung spectral shape for the incident X-rays.

One-dimensional models were computed for 11 logarithmically spaced radii ranging from 6.3×10^9 to 6.3×10^{10} cm. The surface brightnesses of all the lines decrease with radius, but the larger areas of the outer annuli compensate. The optically thick C IV and N V lines are dominated by emission from smaller radii. The model would benefit from better treatments of the two-dimensional character of the illuminated disk structure and the lower boundary condition, a more detailed calculation of electron scattering, and perhaps consideration of departure from hydrostatic equilibrium. It is also important to investigate the sensitivity of the results to the assumed line widths, the assumed illumination angle, and the possible presence of a soft spectral component. Nevertheless, it provides a starting place for interpretation of the line emission.

We assume a distance of 2.0 kpc and reddening $E(B-V) = 0.3$, consistent with the results of the continuum modeling. Table 4 compares the model fluxes with the average emission line fluxes for the 14 FB spectra and four NB spectra of the current campaign and the four HB spectra from 1984. The good agreement between the overall flux levels of the model and observed spectra suggests that reprocessing of X-rays directly illuminating the outer disk can account for the observations. *No strong lines are predicted by the model that do not exist in the observations, and no strong lines are detected in the observations that are not predicted by the model.* The model predicts a flux of 2.6×10^{-12} ergs cm^{-2} s^{-1} during the FB state for the weak C III line at λ1176, but does not predict the C IV line at λ1341.

The intensity ratio of C IV to N V is predicted to be 2.1–2.3,

TABLE 4

AVERAGE EMISSION-LINE FLUXES AND MODEL PREDICTIONS

LINE	FLUX IN LINE (10^{-11} ergs cm^{-2} s^{-1})					
	FB (observed)	FB (model)	NB (observed)	NB (model)	HB (observed)	HB (model)
N V λ1240	0.40	0.36	0.32	0.23	0.13	0.14
O V λ1370	0.08	0.02	0.04	0.01	0.03	0.006
Si IV λ1400	0.10	0.24	0.07	0.12	0.05	0.07
C IV λ1545	0.38	0.77	0.36	0.51	0.18	0.32
He II λ1640	0.06	0.01	0.04	0.003	0.02	0.002
N IV λ1714	0.05	0.03	0.03	0.02	0.02	0.01

while the observed ratios range from 1.0 to 1.4. The enhanced nitrogen abundance inferred from *Einstein* OGS spectra (Kahn et al. 1984) might change this ratio, but the lines are sufficiently optically thick that the abundance dependence is not very strong. A higher temperature in the layers where these ions are found, due perhaps to a smaller line width and therefore smaller escape probability, would also strengthen N V relative to C IV. A nonradiative contribution to the heating might also have this effect. The largest discrepancy between calculated and observed fluxes occurs in the He II line. A very soft component in the illuminating spectrum, which would be expected for X-ray luminosities near the Eddington limit, would probably enhance He II relative to the other lines. The N IV and O V lines connect excited levels, and they are assumed to be optically thin in the model calculation. This assumption is questionable in the inner regions of the disk, but the reasonable level of agreement between measured and predicted ratios of these lines to the optically thick resonance lines suggests that the assumption is adequate.

5. THE REDDENING AND DISTANCE TO SCORPIUS X-1

5.1. *Reddening Estimates*

Applying the average extinction law of Seaton (1979) to combined SWP and LWP spectra taken from the NB state, for successive values of $E(B-V)$ until the strong absorption feature at 2200 Å attributed to interstellar extinction is smoothed out, we derive an $E(B-V)$ of 0.3 ± 0.05. As can be seen from Figure 4 this value gives a very smooth UV continuum and is consistent with the value of 0.35 ± 0.05 derived by Willis et al. (1980) (by fitting the average Galactic extinction law of Nandy et al. 1975 to *IUE* observations of Sco X-1 taken in 1980). Willis et al. were unable to obtain an acceptably smooth UV continuum for their dereddened spectrum, and we suggest this is because the source can change state between the SWP and LWP exposures: it is important to combine an NB or HB state spectrum, since these states change sufficiently slowly that adjacent SWP and LWP may be used with impunity. KRV91 also obtain an $E(B-V)$ of 0.3 using the average Galactic extinction law of Savage & Mathis (1979).

Knude (1987) derives an $E(B-V)$ toward Sco X-1 of 0.11 by using the exceptional extinction curve derived for σ Sco (Bless & Savage 1972) which lies more than 5° from Sco X-1. SFK89 also use the σ Sco extinction curve but include as an additional constraint the He II λ1640 to λ4686 ratio. SFK89 use their low-state value for the flux of λ4686 and an average value of the He II λ1640 fluxes determined by Willis et al. Since both these line features are known to be highly variable, comparing values from widely separated times is at best a risky business. The reported fluxes of the λ1640 line range from 1.6–8.3 (Willis et al. 1980; KRV91; this work), and the reported fluxes of the λ4686 range from 1.1 to 5.2 (Willis et al. 1980; Crampton et al. 1976.

The average Galactic extinction laws can lead to errors of a factor 10 or more for the reddening values at 1300 Å (Mathis 1987) for a particular region of the sky. The region toward Sco X-1 in particular is known to be unusual (Willis et al. 1980; Knude 1987; SFK89) so that even using the extinction curve of σ Sco, lying as it does more than 5° from Sco X-1, is unlikely to provide the correct answer. We conclude that the large deviations in extinction for different lines of sight in the Galaxy (Cardelli & Savage 1988) emphasize the need to measure individual extinction curves.

5.2. *Distance Determination*

In an early study, Crampton et al. (1976) concluded that the distance to Sco X-1 ranged from 1.2 to 2.4 kpc, assuming that the maximum X-ray luminosity corresponded to the Eddington limit, and using reasonable upper and lower limits on the mass of the neutron star of 0.7 and 2.0 $M_\odot$.

Knude (1987) claims a distance of 100–300 pc. However, his study is based on optical photometry of 200 stars all lying within 400 pc: every star in his sample that has a distance greater than 300 pc also has $E(B-V)$ greater than 0.11. Thus Knude's data can only give a lower limit of 300 pc to the distance to Sco X-1. SFK89 derive a distance by assuming that the maximum 2–12 keV flux must yield a luminosity less than the Eddington limit; they quote a flux from Giacconi et al. (1962) and conclude that the distance must be less than 1.4 kpc for Sco X-1. Sco X-1 shows large fluctuations in X-ray luminosity and the highest flux observed by *Ginga* (Hertz et al. 1991) exceeds that observed by Giacconi et al.; hence, their conclusions can be called into question.

Following Penninx (1989, 1990b), we suggest a new method for determining the distance to Sco X-1. Penninx (1989) noted that the ratios of the radio, UV, and X-ray fluxes of these Z sources are very similar and that if we assume that the NB (so defined because this is where the Z sources seem to spend most of their time) is a standard candle, we can determine the relative distances of the Z sources. We further note that at least two models (Lamb 1990; Hasinger et al. 1990) for the Z sources identify the "soft" vertex of the Z as being the point where the X-ray emission from the source is equal to the gravitational pressure of the infalling matter, i.e., the Eddington limit. While the absolute luminosity determined from our UV observations is uncertain at the factor of 2 level, it is consistent with $L_{\rm EDD}$ at the soft vertex. Since the compact object in LMXBs are assumed to be neutron stars, their luminosity at Eddington limit is well defined (a neutron star of 1.4 $M_\odot$ reaches the Eddington limit of solar abundance material at a mass accretion rate of $1.2 \times 10^{-8}\ M_\odot\ {\rm yr}^{-1}$), and their fluxes can indeed be used to determine distances.

Of the six Z sources thus far identified in our Galaxy from X-ray observations, four (GX 17+2, GX 5−1, GX 340+0, and GX 349+2) are known to lie in the Galactic bulge; hence, the distances are considered well known. Scaling from the Z-sources in the Galactic bulge, the implied distance to Cyg X-2 is 8.5 kpc (Penninx 1989), consistent with its fairly well-determined distance of $\approx$8 kpc (Cowley, Crampton, & Hutchings 1979). In Table 5 we show the X-ray, UV, optical, and radio fluxes for Sco X-1 and Cyg X-2 taken when the sources were at the "soft" vertex on the Z. These values are also plotted in a log luminosity versus frequency plot in Figure 8. The ratios of the UV/X-ray and UV/radio are essentially the same within each source; but the radio, UV, and X-ray fluxes of Sco X-1 are $\approx$16 times those of Cyg X-2, implying that the latter is 4 times further away. The implied distance of 2 kpc to Sco X-1 is consistent with the value obtained by Crampton et al. (1976) for a 1.4 $M_\odot$ neutron star.

6. CONCLUSIONS

On the basis of *IUE* observations of Sco X-1 that were simultaneous with X-ray and optical observations taken during the normal and flaring branches, we find that the mass transfer rate for Z-source LMXBs can be determined from the flux level of the optical-ultraviolet spectrum, as determined earlier for Cyg X-2. The simultaneous UV/X-ray observations

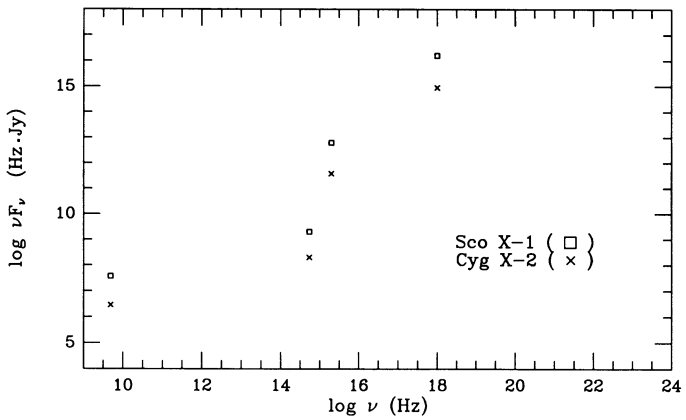

FIG. 8.—A log νF_ν versus log ν plot giving the radio, optical, UV, and X-ray fluxes from the "soft" vertex of the Z for the two sources Sco X-1 and Cyg X-2.

show a direct relationship between the strengths of the UV continuum and line fluxes and the X-ray spectral states.

The observed UV continuum is well represented by the calculated emission from an X-ray–illuminated accretion disk. The mass accretion rate increases monotonically along the Z and ranges from $0.6 \times 10^{-8} M_\odot$ yr^{-1} in the NB state to $1.1 \times 10^{-8} M_\odot$ yr^{-1} in the FB state. The mass accretion rate of the HB state was not observed simultaneously in the UV and X-ray but is assumed to be the lowest calculated from earlier UV observations or $0.4 \times 10^{-8} M_\odot$ yr^{-1}. The best-fit outer disk radius is $(6.3 \pm 0.3) \times 10^{10}$ cm for all three branches; this suggests that the accretion disk fills the Roche lobe of the compact object. The change in UV continuum flux from one branch to another is dependent *only* on the mass accretion rate; since continuum shape and derived disk radius do not vary, we have the first strong evidence that the disk structure is invariant with X-ray spectral state.

Using an average Galactic extinction curve, we derive an $E(B-V)$ of 0.3 ± 0.05 from the 2200 Å absorption feature. However, average Galactic extinction laws can be misleading (since large deviations in extinction have been measured for different lines of sight in the Galaxy) and a conclusive determination of $E(B-V)$ for Sco X-1 requires the measurement of an extinction curve unique to Sco X-1.

Ultraviolet emission lines from He, C, N, O, and Si were detected. The line fluxes vary as a function of X-ray state, with the highest intensities in the FB and the lowest in the NB. A photoionization model, developed to interpret the observed UV emission lines, assumes that a thermal bremsstrahlung X-ray source at 10^8 K with luminosities corresponding to the average mass accretion rates for the FB, NB, and HB states is incident on the accretion disk. The C IV and N V lines which are known from high-resolution *IUE* data to be optically thick (KRV91) are found to be dominated by emission from the outer radii of the disk (around 6.3×10^{10} cm) and the optically thin O V and N IV lines are found to come mainly from smaller radii (around 6.3×10^9 cm). The agreement between the model predictions and the average line fluxes observed are remarkably good and scale appropriately for the three states.

TABLE 5

FLUXES AT SOFT VERTEX OF Z

Source	Radio 4.9 GHz (Jy)	Optical 5500 Å (Jy)	Ultraviolet 1224–1986 Å (Jy)	X-Ray 2–10 keV (Jy)
Cyg X-2.....	6.0×10^{-4}	3.7×10^{-7}	1.9×10^{-4}	9.0×10^{-4}
Sco X-1	7.5×10^{-3}	3.7×10^{-6}	3.1×10^{-3}	1.6×10^{-2}

The X-ray:UV:radio flux ratios of Sco X-1 measured at the lower vertex of the Z in the X-ray color-color diagram are identical with the ratios observed at this point for five other X-ray binaries. The X-ray, UV, and radio fluxes of Sco X-1 are ~16 times those of Cyg X-2 and the other four sources. We suggest that the flux at this vertex, which several theories identify with an accretion rate at the Eddington limit, may be used as a standard candle; the distance to Sco X-1 would then be 2.0 ± 0.5 kpc.

We would like to thank our referee, Günther Hasinger, for a careful reading of the manuscript. The authors would like to acknowledge the many members of the multiwavelength consortium who made this venture possible. We are particularly grateful to Y. Kondo for facilitating observations with the *IUE*. One of the authors (S. D. V.) wishes to thank J. Trümper for hospitality at the Max-Planck-Institut für extraterrestrische Physik during the preparation of this paper. This work was partially supported by NASA grants NAG 5-87 and NAG 528 to the Smithsonian Astrophysical Observatory.

REFERENCES

Begelman, M. C., & McKee, C. 1983, ApJ, 271, 89
Blair, W. P., Raymond, J. C., Dupree, A. K., Wu, C., Holm, A. V., & Swank, J. 1984, ApJ, 278 270
Bless, R. C., & Savage, D. 1972, ApJ, 171, 193
Boggess, A., et al. 1978a, Nature, 275, 372
Boggess, A., et al. 1978b, Nature, 275, 377
Bohlin, R. C., Holm, A. V., Savage, B. D., Snijders, M. A. J., & Sparks, W. M. 1980, A&A, 85, 1
Bruegman, O., & Crenshaw, D. M. 1989, NASA *IUE* Newsletter, 37, 36
Cardelli, J. A., & Savage, B. D. 1988, ApJ, 325, 864
Cowley, A. P., & Crampton, D. 1975, ApJ, 201, L65
Cowley, A. P., Crampton, D., & Hutchings, J. B. 1979, ApJ, 231, 847
Crampton, D., Cowley, A. P., Hutchings, J. B., & Kaat, C. 1976, ApJ, 207, 907
Galeev, A. A., Rosner, R., & Vaiana, G. S. 1979, ApJ, 229, 318
Garcia, M. R. 1987, Ph.D. thesis, Harvard University
Giacconi, R., Gursky, H., Paolini, F. R., & Rossi, B. 1962, Phys. Rev. Letters, 9, 439
Gottlieb, E. W., Wright, E. L., & Liller, W. 1975, ApJ, 195, L33
Hasinger, G. 1987, A&A, 186, 153
Hasinger, G., Priedhorsky, W. C., & Middleditch, J. 1989, ApJ, 337, 843
Hasinger, G., & van der Klis, M. 1989, A&A, 225, 79
Hasinger, G., van der Klis, M., Ebisawa, K., Dotani, T., & Mitsuda, K. 1990, A&A, 235, 131
Hertz, P., et al. 1991, in preparation
Hjellming, R., et al. 1990a, A&A, 235, 147
Hjellming, R., et al. 1990b, ApJ, 365, 681
Howarth, I. D., & Wilson, B. 1983, MNRAS, 202, 347
Kahn, S. M., Seward, F. D., & Chlebowski, T. 1984, ApJ, 283, 286
Kallman, T. R., & McCray, R. 1982, ApJS, 50, 263
Kallman, T. R., Raymond, J. C., & Vrtilek, S. D. 1991, ApJ, 370, 717 (KRV91)
Knude, J. 1987, A&A, 171, 289
Lamb, F. K. 1990, in Proc. 23rd ESLAB Symposium Two Topics in X-ray Astronomy (ESA SP-296), ed. J. Hunt & B. Battrick (Noordwijk: ESA), p. 215
Lyutyi, V. M., & Sunyaev, R. A. 1976, Soviet Astr., 20, 90
Mathis, J. S. 1987, in Exploring the Universe with the *IUE* Satellite, ed. Y. Kondo (Dordrecht: Reidel), p. 517
Mauche, C. W., & Raymond, J. C. 1987, ApJ, 323, 690
Mobasher, B., & Raine, D. J. 1990, MNRAS, 737, 625
Nandy, K., Thompson, F. I., Jamar, C., Monfils, A., & Wilson, R. 1975, A&A, 44, 195
Norris, J. P., & Wood, K. S. 1987, ApJ, 312, 732
Paczyński, B. 1987, Nature, 327, 303
Penninx, W. 1989, in Proc. 23rd ESLAB Symposium Two Topics in X-ray Astronomy (ESA SP-296), ed. J. Hunt & B. Battrick (Noordwijk: ESA), p. 185

Penninx, W., Lewin, W. H. G., Zijlstra, A. A., Mitsuda, K., van Paradijs, J., & van der Klis, M. 1988, Nature, 336, 146
Penninx, W., Lewin, W. H. G., Mitsuda, K., van Paradijs, J., van der Klis, M., & Zijlstra, A. A. 1990a, MNRAS, 243, 114
Penninx, W., Lewin, W. H. G., Tan, J., van Paradijs, J., van der Klis, M., & Mitsuda, K. 1990b, MNRAS, in press
Priedhorsky, W., Hasinger, G., Lewin, W. H. G., Middleditch, J., Parmer, A., Stella, L., & White, N. 1986, ApJ, 306, L91
Pringle, J. E. 1981, ARA&A, 19, 137
Raymond, J. C. 1991, in preparation
Savage, B. D., & Mathis, J. S. 1979, ARA&A, 17, 73
Schachter, J., Filippenko, V., & Kahn, S. M. 1989, ApJ, 340, 1049 (SFK89)
Seaton, M. J. 1979, MNRAS, 187, 73
Shaviv, G., & Wehrse, R. 1986, A&A Letters, 159, 5
Stella, L. 1988, Adv. Space Res., 8, 367
Urry, M., & Reichert, G. 188, *IUE* Newsletter 34
van der Klis, M. 1989, ARA&A, 27, 517
van Paradijs, J., et al. 1991, in preparation
Vrtilek, S. D., Raymond, J. C., Garcia, M. R., Verbunt, F. W., & Hasinger, G. R. 1990, A&A, 235, 162
Vrtilek, S. D., Penninx, W., Verbunt, F., & Raymond, J. 1989, in Proc. 23rd ESLAB Symposium on Two Topics in X-ray Astronomy (ESA SP-296), ed. J. Hunt & B. Battrick (Noordwijk: ESA), p. 215
Willis, A. J., et al. 1980, ApJ, 237, 596